The Astrophysical Journal, 745:77 (10pp), 2012 January 20 doi:10.1088/0004-637X/745/1/77
© 2012. The American Astronomical Society. All rights reserved. Printed in the U.S.A.

A PHOTOCHEMICAL MODEL FOR THE CARBON-RICH PLANET WASP-12b

Ravi kumar Kopparapu[1,3], James F. Kasting[1,3], and Kevin J. Zahnle[2]
[1] Department of Geosciences, Penn State University, 443 Deike Building, University Park, PA 16802, USA
[2] NASA Ames Research Center, MS 245-3, Moffett Field, CA 94035, USA
Received 2011 March 17; accepted 2011 October 11; published 2011 December 29

ABSTRACT

The hot-Jupiter WASP-12b is a heavily irradiated exoplanet in a short-period orbit around a G0-star with twice the metallicity of the Sun. A recent thermochemical equilibrium analysis based on *Spitzer* and ground-based infrared observations suggests that the presence of CH_4 in its atmosphere and the lack of H_2O features can only be explained if the carbon-to-oxygen ratio in the planet's atmosphere is much greater than the solar ratio ([C]/[O] = 0.54). Here, we use a one-dimensional photochemical model to study the effect of disequilibrium chemistry on the observed abundances of H_2O, CO, CO_2, and CH_4 in the WASP-12b atmosphere. We consider two cases: one with solar [C]/[O] and another with [C]/[O] = 1.08. The solar case predicts that H_2O and CO are more abundant than CO_2 and CH_4, as expected, whereas the high [C]/[O] model shows that CO, C_2H_2, and HCN are more abundant. This indicates that the extra carbon from the high [C]/[O] model is in hydrocarbon species. H_2O photolysis is the dominant disequilibrium mechanism that alters the chemistry at higher altitudes in the solar [C]/[O] case, whereas photodissociation of C_2H_2 and HCN is significant in the super-solar case. Furthermore, our analysis indicates that C_2H_2 is the major absorber in the atmosphere of WASP-12b and the absorption features detected near 1.6 and 8 μm may be arising from C_2H_2 rather than CH_4. The *Hubble Space Telescope's* WFC3 can resolve this discrepancy, as C_2H_2 has absorption between 1.51 and 1.54 μm, while CH_4 does not.

Key word: planetary systems

Online-only material: color figures, machine-readable table

1. INTRODUCTION

The discovery of the first transiting planet, HD 209458b (Charbonneau et al. 2000; Henry et al. 2000), opened up a new window to observe and study extrasolar planetary systems. By combining transit data with radial velocity measurements, one can determine the mass and radius of a transiting planet (Mazeh et al. 2000; Laughlin et al. 2005a, 2005b; Holman & Murray 2005; Agol et al. 2005). Apart from these physical properties of the planet, it has also been shown that the transmission and emission spectra from ground- and space-based observations can be used to place constraints on the atmospheric composition (Charbonneau et al. 2002; Vidal-Madjar et al. 2003, 2004; Tinetti et al. 2007; Snellen et al. 2008; Swain et al. 2009a, 2009b), brightness temperature (Deming et al. 2005; Charbonneau et al. 2005), and even day–night temperature contrast (Knutson et al. 2007) of transiting planets. To date, most of the planets discovered are "hot Jupiters" (Collier-Cameron 2002), but recently terrestrial mass planets have also been discovered (Léger et al. 2009; Charbonneau et al. 2009).

The observational determination of chemical species that exist in the outer atmospheric layers of transiting planets provides us with an opportunity to investigate the underlying chemistry. Typically, thermochemical equilibrium has been assumed in models of exoplanet atmospheres (Burrows et al. 1997; Fortney et al. 2005; Seager et al. 2005; Marley et al. 2007; Madhusudhan et al. 2011a). This is a good assumption at the high temperatures and high pressures prevailing in the lower layers of close-in gas giants. Disequilibrium caused either by the UV flux of the host star (photochemistry) or by eddy and molecular diffusion (vertical transport) has been considered in some models (Liang et al. 2003; Cooper & Showman 2006; Zahnle et al. 2009a, 2009b; Line et al. 2010; Moses et al. 2011). These studies showed that disequilibrium mechanisms can be significant in determining the chemical composition of hot Jupiters.

Here, we investigate the significance of photochemistry and transport in determining the abundances of major species, H_2O, CO, and CH_4, observed in the dayside thermal emission spectrum (Madhusudhan et al. 2011a; Croll et al. 2011) of the transiting hot-Jupiter WASP-12b (Hebb et al. 2009). At the time of its discovery, WASP-12b was the most highly irradiated exoplanet ($T > 2500$ K) with the largest radius (1.79 R_J) and the shortest orbital period (1.09 days). Recently, Madhusudhan et al. (2011a) reported that *Spitzer Space Telescope* observations show strong absorption features of CH_4 in the 3.6 μm channel and CO in the 4.5 μm channel, whereas weaker features were observed in the 5.8 μm channel where H_2O absorbs. This suggests that CH_4 and CO are dominant and that H_2O is less abundant in the atmosphere of WASP-12b. Assuming equilibrium chemistry and solar [C]/[O] = 0.54, H_2O and CO should be the dominant species and CH_4 and CO_2 should be the least abundant. Therefore, a solar [C]/[O] ratio is ruled out. Madhusudhan et al. (2011a) conclude that to explain the observed abundance of CH_4 and CO, WASP-12b must have [C]/[O] $\geqslant 1$, implying that it is a carbon-rich planet.

WASP-12b is one of the most highly irradiated known exoplanets, so photochemistry could play an important role in determining its atmospheric composition. Assuming [C]/[O] = 1, analysis of observations using equilibrium chemistry models suggests mixing ratios (with respect to molecular hydrogen) less than 10^{-7} for H_2O, greater than 10^{-4} for CO, $\sim 10^{-5}$ for CH_4, and less than 10^{-9} for CO_2. Our goal in this study is to examine how the vertical distribution and abundances of these species are affected by photochemistry. Specifically, we wish

[3] Virtual Planetary Laboratory.

Table 1
Reaction List and Rate Constants (K. Zahnle 2010, private communication) Used in This Study

Number	Reactants		Products	Rate[a]	Reference
1	H + H + M	→	H_2 + M	$8.8 \times 10^{-33}(T/298)^{-0.60}$	Baulch et al. (1992)
	H + H	→	H_2	1.0×10^{-12}	
2	O + H + M	→	OH + M	4.3×10^{-32}	Tsang & Hampson (1986)
	O + H	→	OH	1.0×10^{-12}	
3	H_2 + O	→	OH + H	$3.5 \times 10^{-13}(T/298)^{2.67}e^{-3160/T}$	Baulch et al. (1992)
4	H+ OH + M	→	H_2O + M	$6.6 \times 10^{-32}(T/298)^{-2.1}$	Javoy (2003)
	H+ OH	→	H_2O	$2.7 \times 10^{-10}e^{-75/T}$	Cobos & Troe (1985)
5	H_2+ OH	→	H_2O + H	$1.6 \times 10^{-12}(T/298)^{1.60}e^{-1660/T}$	Baulch et al. (1992)

Notes. Only the forward rate constants are given as we calculate reverse rate constants from the forward rate assuming thermodynamic equilibrium (see the discussion in Section 2). For three-body reactions, the first and second row represent the low- and high-pressure rate limits, respectively.

[a] Two-body reaction rates are in $cm^3\ s^{-1}$; three-body rates are in $cm^6\ s^{-1}$.

(This table is available in its entirety in a machine-readable form in the online journal. A portion is shown here for guidance regarding its form and content.)

to determine whether photochemical models make qualitatively different predictions from those of thermochemical equilibrium models. We consider two cases, one with solar [C]/[O] = 0.54 and another with [C]/[O] = 1.08, both of which have also been studied with equilibrium models.

2. MODEL DESCRIPTION

We use a one-dimensional photochemical model initially developed to study primitive terrestrial atmospheres (Kasting 1982, 1983; Zahnle 1986; Kasting 1990). The model has been modified to suit the hot-Jupiter temperature regime by including "backward" chemical reactions that do not occur at the low temperatures and pressures encountered in Earth's atmosphere (Line et al. 2010; Moses et al. 2011). This model solves a set of nonlinear, coupled ordinary differential equations for the mixing ratios of all species at all heights using the reverse Euler method. The method is first order in time and uses second-order centered finite differences in space. We include the following 31 chemical species involved in 230 reactions: O, O_2, H_2O, H, OH, CO_2, CO, HCO, H_2CO, CH_4, CH_3, CH_3O, CH_3OH, CH, CH_2, H_2COH, C, C_2, C_2H, C_2H_2, N, N_2, NH, NH_2, NH_3, CN, HCN, H_2, He, $O(^1D)$, and $^1CH_2$. These species are divided into long-lived species (from O to H_2), short-lived species ($O(^1D)$ and $^1CH_2$), and "inert" species (He). Both chemistry and vertical transport by eddy diffusion are considered for long-lived species, whereas transport is neglected for short-lived species. Constant mixing ratios with altitude are assumed for "inert" species. The reaction list and rate constants were obtained from K. Zahnle (2010, private communication) and are listed in Table 1. We have taken only the "forward" reactions and corresponding rate coefficients, k_f, from K. Zahnle (2010, private communication): the reverse rate coefficients, k_r, at each temperature level (grid) were calculated assuming thermodynamic equilibrium: $k_r = k_f/k_{eq}$, where k_{eq} is the equilibrium constant for the reaction and is given by $k_{eq} = e^{\Delta G^\circ/RT}$. Here ΔG° is the change in the Gibbs free energy for the reaction and is calculated from the Gibbs free energy of formation of reactants and products obtained from NIST-JANAF thermochemical tables when available[4] (and from NASA thermobuild Web site[5] when not available): $\Delta G^\circ = \Delta G^\circ_f(\text{reactants}) - \Delta G^\circ_f(\text{products})$. However, it should be noted that one cannot simply calculate k_r as discussed above. This is because the rate coefficients are given in units applicable to number densities whereas the thermodynamic quantities (enthalpy, entropy, and Gibbs energies) are calculated at a reference pressure (usually 1 bar). For reactions that have different number of reactants and products, proper pressure terms must be added to obtain accurate rate coefficients. We have appropriately included these terms in our reverse rates. Discussion of these correction terms is given in Section 2.2 of Visscher & Moses (2011).

As lower boundary conditions, we fix the mixing ratios of the species at thermodynamic equilibrium values. Constant (zero) deposition velocities are assumed for the other species. The upper boundary condition is set to zero flux for all the long-lived species. A more detailed description of the numerical scheme employed in this model is given in Pavlov et al. (2001).

The vertical grid has 100 altitude levels, ranging from 0 km (lower boundary) to 12,800 km (upper boundary) in 128 km increments. The lower boundary pressure is set at 1 bar and the upper boundary is fixed at 10^{-8} bar. Going to higher pressures is unnecessary, because the species profiles are already close to thermodynamic equilibrium well above the 1 bar level. For the temperature profile, we use one of the best-fit models from Madhusudhan et al. (2011a) which has no inversion (purple curve in their Figure 1). The pressure profile was recalculated from this temperature profile by assuming hydrostatic equilibrium and using the calculated mean molecular weights from the photochemical model. Vertical transport is parameterized as eddy diffusion, as is common in one-dimensional photochemical models. The dayside eddy diffusion profile from Figure 1 of Line et al. (2010), which is originally obtained from the vertical winds from HD 189733b GCM of Showman et al. (2009), is adopted. We have also performed sensitivity tests by varying eddy profiles, as discussed in Section 4. Both the temperature and eddy profiles in our photochemical model are shown in Figure 1.

For comparative purposes, we also calculate the thermodynamic equilibrium mixing ratios for all the species in the photochemical model at each altitude by solving simultaneously a system of chemical equilibrium equations. These equations require the total elemental abundances of carbon, oxygen, hydrogen, and nitrogen (as we consider only compounds from these elements) and Gibbs free energies as a function of temperature. Solar elemental abundances from Asplund et al. (2005)

[4] http://webbook.nist.gov/chemistry/
[5] http://www.grc.nasa.gov/WWW/CEAWeb/ceaThermoBuild.htm

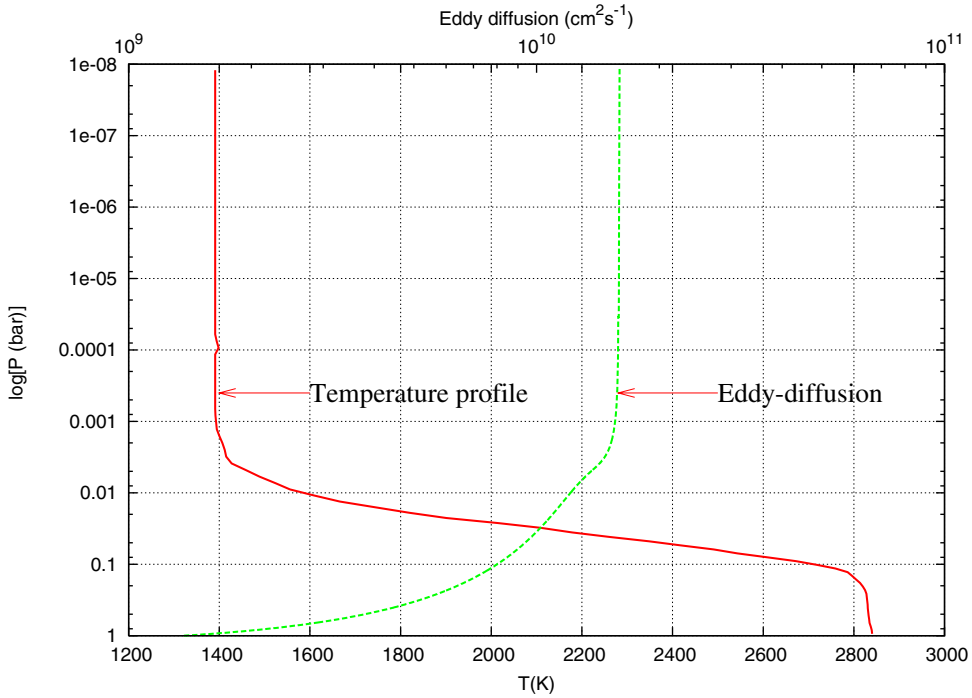

Figure 1. Temperature profile (red solid curve) and eddy diffusion profile (green dashed line) used in our photochemical model. The temperature profile is taken from one of the models of Madhusudhan et al. (2011a) with no inversion, as a profile with inversion is ruled out by the data. This profile is then recalculated using hydrostatic equilibrium to be consistent with our photochemical model. Eddy diffusion profile is taken from the dayside profile of Line et al. (2010).
(A color version of this figure is available in the online journal.)

are assumed to be our base values, but we report results for both solar [C]/[O] and 2× solar [C]/[O]. To calculate Gibbs free energies, the enthalpy of formation at the reference temperature (298 K) and entropy are needed. We then use the expressions given in Chase (1998, p. 16) to calculate Gibbs free energy of formation for each species.

We initially tested our model by attempting to reproduce the results of Line et al. (2010) for the hot-Jupiter planet HD189733b. The dayside temperature and eddy diffusion profiles were taken from their Figure 1. The lower boundary pressure was fixed at 10 bar. Both the thermochemical equilibrium and photochemical model results are shown in Figure 2 and are in good agreement with the similar analyses of Line et al. (2010) and Moses et al. (2011). Moreover, our model maintains equilibrium concentrations for all the major species in the deeper levels (∼10 bar), as it should at high temperatures and pressures.

The star WASP-12 is a G0 star[6] with an effective temperature of 6350 K and twice the solar metallicity (Hebb et al. 2009). To simulate its spectrum, we used a G0V star spectrum from Pickles' stellar spectral flux library (Pickles 1998),[7] normalized to a solar flux of 1360 W m^{-2} (the value at Earth's orbit today). We then multiplied the flux at each wavelength by a value consistent with inverse square law of the distance to get the correct flux for WASP-12b. The Pickles spectra are normalized to 1 at 5556 Å. The fluxes from this dimensionless model spectrum are converted to W m^{-2} nm^{-1} by multiplying the following flux expression from Gray (1992):

$$\log F_{5556} = -0.40V - 8.449, \quad (1)$$

where F_{5556} is the flux at 5556 Å and V is the visual magnitude of the star. For WASP-12, $V = 11.69$ (Hebb et al. 2009). In Figure 3, we show the G0V star spectrum along with F2V and the Sun. A fixed stellar zenith angle of 50° is assumed in all our models, the same value that is used in our models of Earth's atmosphere (e.g., Pavlov et al. 2001). This value is close to the value of 48° used by Moses et al. (2011) to reproduce secondary transit spectra in the atmosphere of HD 189733b.

3. RESULTS

We consider two different cases. In the first, we assume [C]/[O] = 0.54 (solar) and in the second we assume [C]/[O] = 1.08 (twice solar). Figure 4 shows mixing ratio profiles of some of the major species in our model, plotted against pressure for solar [C]/[O] abundance. The lower boundary in both the models is kept at 1 bar pressure ($T = 2841$ K) as the observed spectral features mostly arise from pressures equal to or less than the 1 bar level (Fortney et al. 2005; Tinetti et al. 2007; Swain et al. 2009a; Madhusudhan et al. 2011a). Dashed lines represent the profile obtained from equilibrium chemistry, solid lines from our photochemical model, and filled squares represent mixing ratios of respective species at the lower boundary.

In the case of solar [C]/[O] (Figure 4), most of the oxygen and carbon is in H_2O and CO. The chemical loss timescale (τ_{chem}) for H_2O, CO, and CO_2 is smaller than the transport timescale (τ_{trans}); hence, as altitude increases, the abundances stay at their equilibrium values until $\sim 10^{-5}$ bar (Prinn & Barshay 1977). Below this pressure level (i.e., at higher altitudes) H_2O gets photolyzed. H_2O photolyzes at lower altitudes than does CO because the dissociation energy for H_2O (5.17 eV) is lower than that of CO (11.14 eV) (Yung & DeMore 1999, Table 2.4). To break this strong C–O bond, photons of wavelength $\leqslant 111.3$ nm are needed (H_2O needs photons of

[6] http://www.superwasp.org/wasp_planets.htm
[7] http://cdsarc.u-strasbg.fr/viz-bin/Cat?J/PASP/110/863

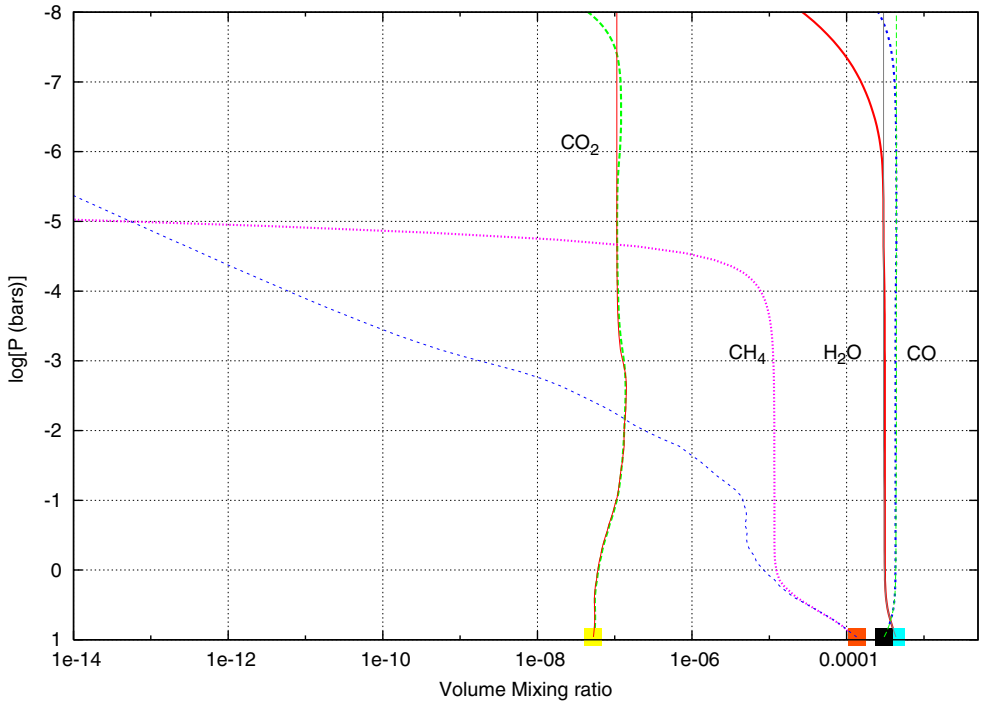

Figure 2. Photochemical mixing ratio profiles of H_2O, CO, CH_4, and CO_2 derived from our model of the dayside atmosphere of HD 189733b. For comparison, see Line et al. (2010) and Moses et al. (2011).

(A color version of this figure is available in the online journal.)

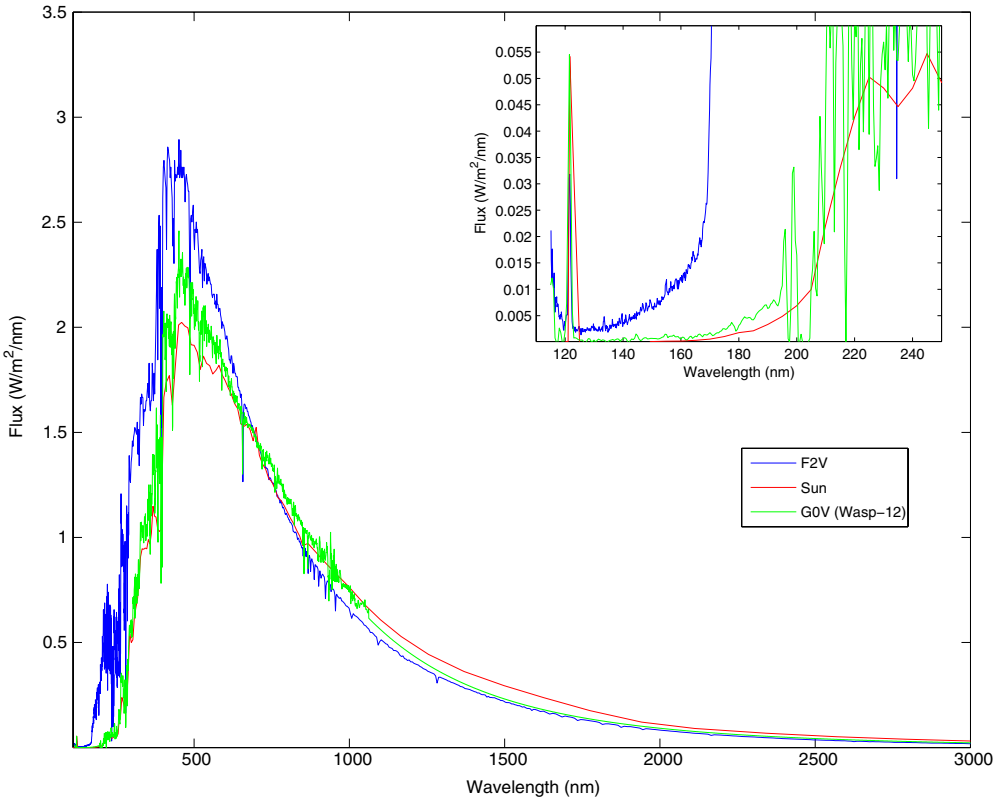

Figure 3. Comparison of the normalized flux of a G0V stellar spectrum from Pickles' (1998) stellar flux library (green curve), which is assumed for the star WASP-12, with an F2V star (top blue curve) and the Sun (red bottom curve). Inset figure shows the UV region.

(A color version of this figure is available in the online journal.)

wavelength $\lesssim$ 239.8 nm to break its bond). CO photolysis is not simulated in our photochemical model and it can be a source of carbon and oxygen photochemistry at high altitudes (Line et al. 2010; Moses et al. 2011), but it should be relatively slow because of the small number of photons at these short wavelengths. By contrast, the photon flux is quite high at the longer wavelengths that can photolyze H_2O (green curve in Figure 3 inset).

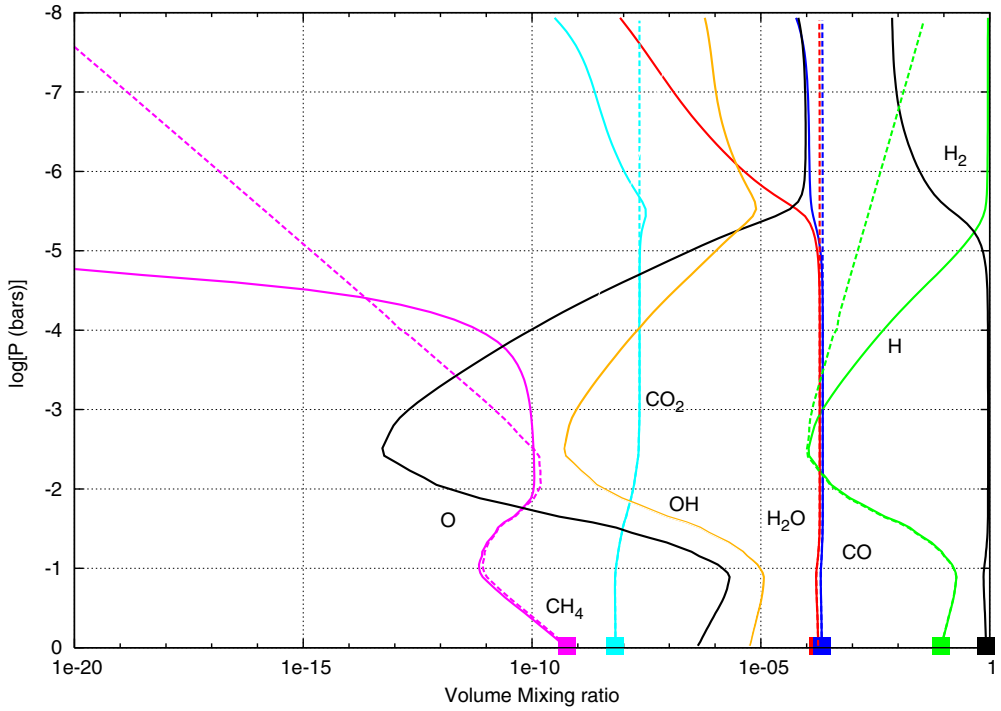

Figure 4. Equilibrium (dashed) and photochemical (solid) mixing ratio profiles of major species, for [C]/[O] = 0.54 (the solar value). Filled squares represent equilibrium values at the lower boundary. The mixing ratios refer to volume mixing ratio. The helium abundance is 0.07836.
(A color version of this figure is available in the online journal.)

In the case of CO_2, the equilibrium abundance is maintained until 10^{-5} bar and is set by the following kinetic reactions that transfer oxygen from CO and H_2O to CO_2:

$$H_2O + H \leftrightarrow H_2 + OH \quad (2)$$

$$CO + OH \leftrightarrow CO_2 + H. \quad (3)$$

At altitudes above 10^{-5} bar, H_2O photolysis becomes the dominant source of OH production. The OH then combines with CO through Equation (3) to produce excess CO_2 (local maximum of solid light-blue curve $>10^{-5}$ bar). Above this level, CO_2 becomes less abundant because it is itself photolyzed.

The shape of the equilibrium profile for CH_4 can be understood from the following reaction:

$$CO + 3H_2 \leftrightarrow CH_4 + H_2O \quad (4)$$

and the corresponding equilibrium constant:

$$K_{eq} = \frac{p_{CH_4} p_{H_2O}}{p_{CO} p_{H2}^3}, \quad (5)$$

where "p_i" represents the partial pressure of species i. The partial pressure is related to the total pressure and volume mixing ratio as $p_i = f_i P$. As pressure increases (going downward) from 10^{-8} bar, the denominator term on the right-hand side of Equation (5) increases. Temperature is constant in this region (see Figure 1), as is the H_2O/CO ratio. Thus, in order to maintain equilibrium CH_4 must increase with depth. Below 10^{-2} bar, the temperature starts to increase with depth. CH_4 is more stable at lower temperatures and is also more sensitive to temperature changes than other species. Hence, it becomes less abundant in the 10^{-2} to 10^{-1} bar regime. At pressures above 10^{-1} bar, the temperature again remains constant, so CH_4 must again increase with depth as it does in the upper atmosphere.

The CH_4 profile from the photochemical model (solid magenta curve in Figure 4) follows the equilibrium profile at pressures up to $\approx 10^{-2}$ bar. Above this level, $\tau_{chem} \sim \tau_{trans}$ (quench level) and CH_4 remains well mixed near its equilibrium value of 10^{-10}. Photolysis of CH_4 occurs above 10^{-3} bar (see Figure 5) mainly through the following reactions:

$$CH_4 + h\nu \rightarrow CH_2 + 2H, \quad (6)$$

$$CH_4 + h\nu \rightarrow CH_3 + H, \quad (7)$$

$$CH_4 + h\nu \rightarrow {}^1CH_2 + H_2. \quad (8)$$

Although H is produced through CH_4 photolysis, it is not enough to explain the increase in H abundance between 10^{-2} and 10^{-3} bar (light-blue solid curve in Figure 4). This increase in H is mainly due to the production of OH through H_2O photolysis at this level, which then combines with the most abundant molecule in this atmosphere, H_2, through the reverse of reaction (2):

$$H_2O + h\nu \rightarrow H + OH, \quad (9)$$

$$H_2 + OH \rightarrow H_2O + H. \quad (10)$$

As the OH abundance increases, more H_2 is consumed and its mixing ratio decreases above 10^{-5} bar (solid black curve in Figure 4). Eventually, H_2O itself becomes depleted by photolysis, so the production of OH radical diminishes. At this point, H_2 asymptotically reaches a mixing ratio of 10^{-2}. The increase in H also affects the atomic oxygen abundance (black solid curve in Figure 4) by the following reaction:

$$CO + H \rightarrow O + CH. \quad (11)$$

Note that CO photolysis, which is not included in our model, may dominate the above reaction in producing atomic oxygen.

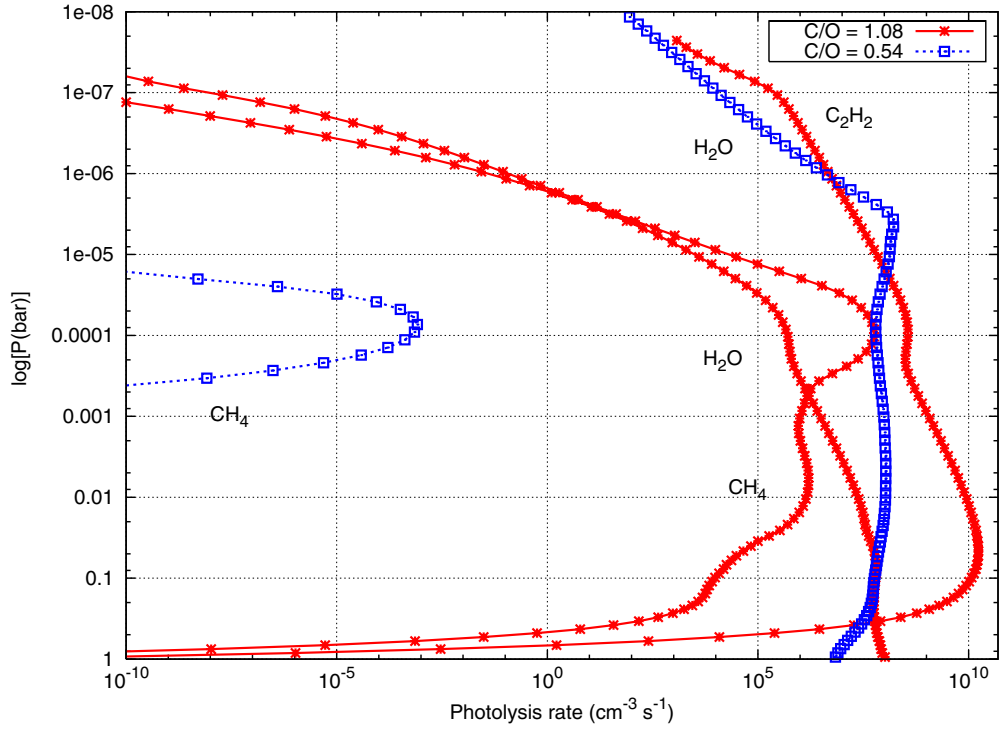

Figure 5. Photolysis rates of H_2O and CH_4 for [C]/[O] = 0.54 (dashed, solar) and [C]/[O] = 1.08 (solid, super-solar) including C_2H_2.
(A color version of this figure is available in the online journal.)

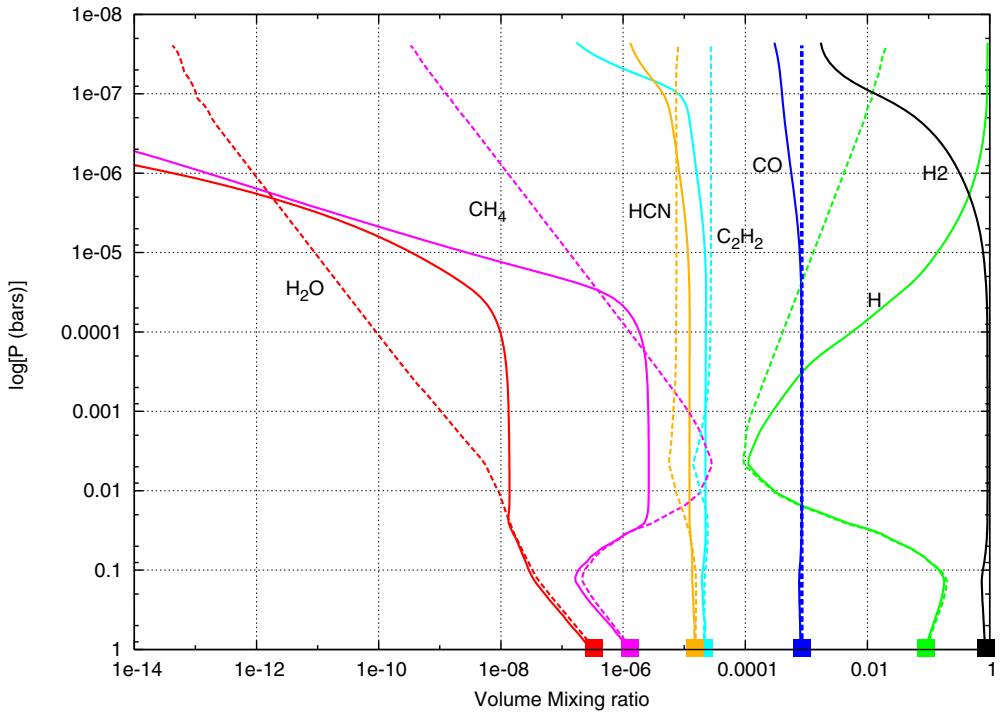

Figure 6. Mixing ratio profiles from equilibrium (dashed) and photochemical (solid) models for [C]/[O] = 1.08 (twice solar).
(A color version of this figure is available in the online journal.)

Our analysis shows that, in the [C]/[O] = 0.54 case, the abundances of major species (Figure 4) in WASP-12b's atmosphere are mainly determined by thermochemical equilibrium, with departures at high altitudes due to disequilibrium chemistry driven by H_2O photolysis. This is not surprising considering that H_2O is far more abundant than CH_4. The photolysis rates of H_2O and CH_4 as a function of pressure (altitude) for solar (blue) and super-solar (red) [C]/[O] are shown in Figure 5. In the solar case, at any given height, H_2O is more rapidly photodissociated than is CH_4, as it is more abundant. In the super-solar [C]/[O] case (Figure 6), C_2H_2 is more abundant than either H_2O or CH_4, and so it is photolyzed more rapidly at high altitudes.

Madhusudhan et al. (2011a) report that the spectrum obtained from the dayside multi-wavelength photometry of WASP-12b

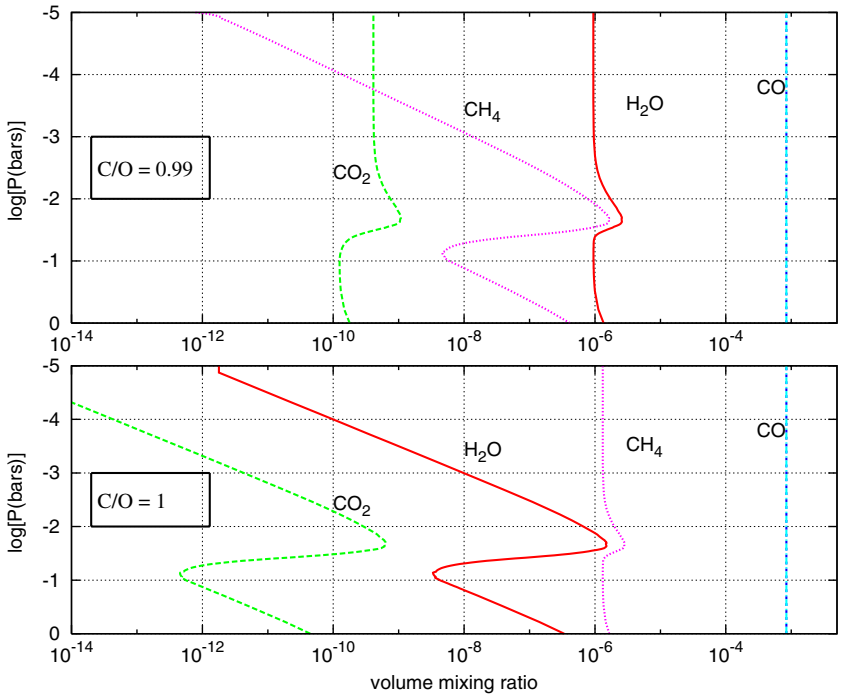

Figure 7. Diagrams showing the rapid shift in species' concentrations as C/O increases from 0.99 (top panel) to 1.0 (bottom panel).
(A color version of this figure is available in the online journal.)

is best explained if one assumes [C]/[O] $\geqslant$ 1, using chemical equilibrium models. Under this assumption, the atmosphere is depleted in H_2O, enhanced in CH_4, and rich in CO. These equilibrium model profiles (dashed lines), along with our photochemical model results, for [C]/[O] = 1.08 are shown in Figure 6. In contrast to the solar [C]/[O] model, most of the oxygen is now in CO (blue solid line), and CH_4 (magenta curve) is more abundant than H_2O (red curve). The switchover from an atmosphere where H_2O and CO are the dominant species to one in which CH_4 and CO become abundant happens precisely at [C]/[O] = 1. This transition is illustrated in Figure 7.

In Figure 6, the abundance of H_2O follows the equilibrium profile at pressures up to about 10^{-2} bar in the [C]/[O] = 1.08 model. At that point, transport by eddy diffusion becomes faster than the chemical reaction timescale, so the equilibrium value is maintained until $\sim 10^{-4}$ bar. Photolysis begins above this level and the abundance of H_2O decreases. The behavior of CH_4 is similar to the solar [C]/[O] case, though it is relatively more abundant in this high [C]/[O] model. Note that for CH_4 and H_2O, the photochemical mixing ratios are not exactly equal to the equilibrium values below 0.1 bar. The reason is as follows. At high altitudes (above 10^{-6} bar), atomic hydrogen (green solid curve in Figure 6) becomes a dominant species (more than H_2). Our photochemical model uses a minor constituent approximation for the diffusion coefficient in a binary mixture (Equation (15.29), Banks & Kockarts 1973), which clearly is not applicable to H at this level. Due to this approximation, the mixing ratio of H exceeds unity above 10^{-6} bar, which is unphysical. Therefore, we renormalize the mixing ratios of each species in our photochemical model so that they sum to unity, and hence the equilibrium and photochemical profiles deviate slightly in the lower atmosphere. Note that this should not affect our conclusions in any way regarding which species are dominant (discussed in the next paragraph) in Wasp-12b's high [C]/[O] model.

As can be seen from Figure 6, and also pointed by J. Moses et al. (2011, private communication), the dominant hydrogen species (apart from H and H_2) in this model are HCN and C_2H_2. Therefore, the photolysis of these two species drives the disequilibrium chemistry in the upper atmosphere. For example, in the solar model, the catalytic H_2 destruction mechanism initiated by H_2O photolysis (Equations (9) and (10)) was used to explain the increase in H abundance shown in Figure 4 (green solid curve). A similar increase of H at high altitudes can be noticed in the high [C]/[O] case. Reactions (9) and (10) require OH production through H_2O photolysis, which is negligible in the high [C]/[O] model. Instead, the following reactions are important:

$$C_2H_2 + h\nu \rightarrow C_2H + H, \quad (12)$$

$$C_2H + H_2 \rightarrow C_2H_2 + H, \quad (13)$$

$$HCN + h\nu \rightarrow CN + H, \quad (14)$$

$$CN + H_2 \rightarrow HCN + H. \quad (15)$$

The results of these reactions can be seen in Figure 6. At altitudes above $\sim 10^{-2}$ bar, the photolysis of C_2H_2 and HCN produces C_2H, CN, and H through the above reactions. An increase in H can be seen as a result. The abundances of CN and C_2H are not large enough below 10^{-5} bar to have a significant effect on the mixing ratio of H_2. Above this level, reactions (13) and (15) result in the decrease of H_2 mixing ratio (solid black line in Figure 6) and corresponding increase of H. Further up, C_2H_2 and HCN become scarce and the production of C_2H and CN diminishes, which in turn reduces the rate of production of H. Therefore, H assumes a nearly constant mixing ratio thereafter.

Based on their thermodynamic equilibrium calculations, Madhusudhan et al. (2011a) concluded that Wasp-12b is abundant in CH_4 and deficient in H_2O. Our analysis indicates

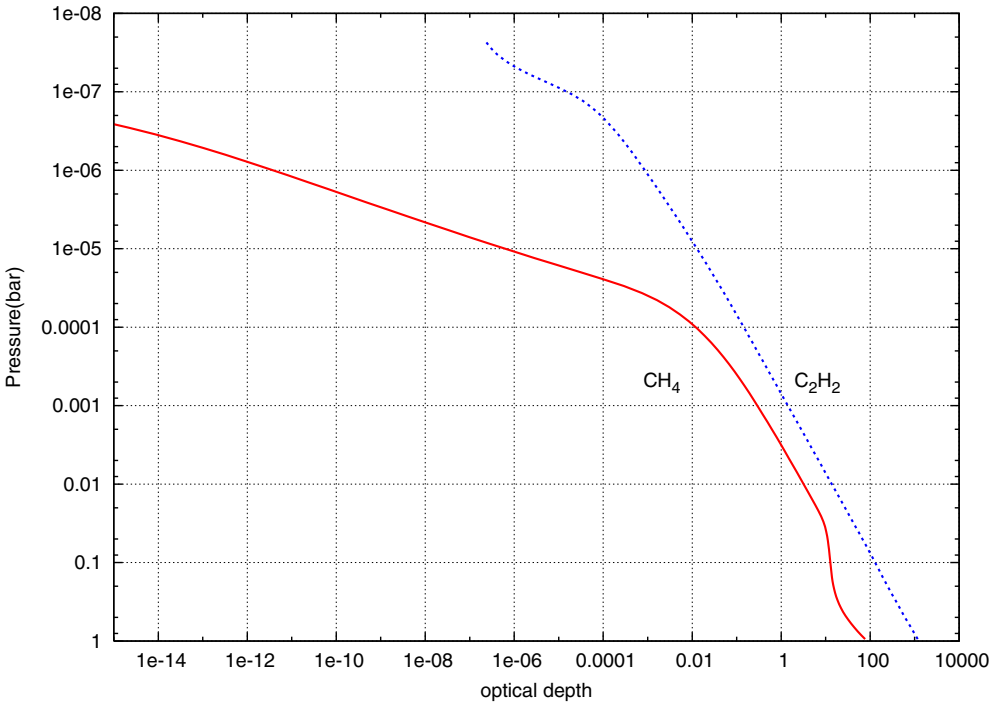

Figure 8. Approximate optical depths of the CH_4 7.7 μm band (red solid) and the C_2H_2 7.5 μm band (blue dashed) as a function of pressure. The optical depth of C_2H_2 is larger than CH_4 indicating that it may be the major absorber in WASP-12b's atmosphere.
(A color version of this figure is available in the online journal.)

that both the equilibrium and photochemical models predict C_2H_2 and HCN are more abundant than CH_4. Also, C_2H_2 has strong absorption in the range 2.98–3.1 μm and also between 7.2 and 7.9 μm, whereas CH_4 has absorption features between 3.2–3.45 μm and 7.3–8 μm. The short wavelength range for C_2H_2 has little overlap with the *Spitzer* 3.6 μm channel[8] but the longer wavelength range for both species overlaps with *Spitzer's* 8 μm channel.[9] In order to determine which is the dominant absorber, we have calculated the optical depths of the C_2H_2 7.5 μm band and the CH_4 7.7 μm band as a function of pressure, as shown in Figure 8. Approximate band-averaged absorption coefficients for these features are 2×10^{-19} cm^2 and 4×10^{-19} cm^2, respectively.[10] The column depths are taken from our photochemical model. Clearly, C_2H_2 has a larger optical depth than CH_4 and is the dominant absorber. Note that, Madhusudhan et al. (2011a) point out that 0.01–1 bar pressure levels contribute most to the observed spectrum and that C_2H_2 is considerably more abundant than CH_4 within this pressure range (Figure 6). Therefore, future analysis of observations of carbon rich planets (including further analysis of WASP-12b) should consider higher-hydrocarbon species.

4. DISCUSSION

Our analysis confirms the previous thermodynamic equilibrium result that [C]/[O] $\geqslant 1$ is needed to explain the observed overabundance of CH_4 in the atmosphere of WASP-12b. A similar conclusion was reached by Line et al. (2010) but for a different hot-Jupiter planet, HD 189733b. These authors varied [C]/[O] from 0.1 to 10 times the solar value, while keeping the total metallicity at the solar value (Figure 6 in their paper), and examined the effect on thermochemcal equilibrium mixing ratios at the lower boundary. As [C]/[O] increases, most of the carbon in their model is in CO and CH_4. At [C]/[O] = 1, H_2O and CH_4 switch their profiles just as they do in our equilibrium models of WASP-12b (Figure 7). Although our equilibrium models agree qualitatively with theirs, the respective mixing ratios of the major species differ because of different elemental abundances and overall hotter temperatures (their ~1500 K versus our 2800 K).

We have also performed a sensitivity test to eddy diffusion varying by three orders of magnitude above and below our eddy profile. For the larger case the species concentrations are well mixed over much of the atmosphere, deviating from the equilibrium even at relatively low altitudes (~0.1 bar). Consequently, the photolysis of C_2H_2 and HCN is not effective in producing atomic hydrogen (as mixing dominates photolysis even at high altitudes). On the other hand, if the eddy diffusion coefficient is small (as proposed by Youdin & Mitchell 2010), mixing is not effective and photochemistry becomes important at mid altitudes (10^{-3} to 10^{-4} bar). Therefore, significant deviations from equilibrium occur at all altitudes above this level.

4.1. A Possible Mechanism for the Origin of Excess Carbon in WASP-12b

The high [C]/[O] ratio in WASP-12b is unexpected, considering that the host star has a solar [C]/[O] ratio (see Fossati et al. 2010, Table 2). In the standard core accretion model (Pollack et al. 1996), volatiles such as carbon and oxygen are expected to remain unfractionated in forming giant planets (Owen et al. 1999). Lodders (2004) pointed out that *Galileo* probe measurements of Jupiter's atmosphere show an enriched carbon abundance of 1.7 times solar and a depletion of oxygen by a factor of four (but see further discussion below). To explain

[8] Band pass range from 3.08 to 4.01 μm: http://irsa.ipac.caltech.edu/data/SPITZER/docs/irac/calibrationfiles/spectralresponse/
[9] Band pass range from 6.15 to 10.49 μm: http://irsa.ipac.caltech.edu/data/SPITZER/docs/irac/calibrationfiles/spectralresponse/
[10] http://vpl.astro.washington.edu/spectra/c2h2pnnlimagesmicrons.htm

this result, Lodders (2004) proposed a model in which carbonaceous matter began to condense in the solar nebula beyond 5 AU, thereby providing the increased mass density needed for rapid core growth. By contrast, in the standard accretion model, Jupiter forms just beyond the "ice line" where water ice begins to condense. In the Lodders (2004) model, the ice line would have been farther out, beyond the orbit of Jupiter, and this would explain Jupiter's apparent deficiency in O relative to C. A similar mechanism might then account for the high [C]/[O] ratio in WASP-12b.

Although the Lodders (2004) model could be correct, we suspect that Jupiter formed beyond the ice line, with a solar [C]/[O] ratio, and that other factors are responsible for observed [C]/[O] enrichments in exoplanets. The *Galileo* probe is widely thought to have descended into an infrared "hot spot" (Atreya et al. 1999), that is, an area of downwelling air that had been depleted in H_2O during its uplift from below. In support of this idea, the H_2O mixing ratio was observed to gradually increase with depth down to 20 bars, at which point the probe lost contact with Earth (see Atreya et al. 1999, Table 1). Furthermore, thunderstorms and lightning were also observed by the probe deeper than 4–5 bars (Gierasch et al. 2000; Ingersoll et al. 2000; Atreya et al. 2005), which is consistent with equilibrium cloud condensation models which predict that water clouds can form in this pressure range if the oxygen abundance is at least solar (Atreya et al. 2005).[11]

As an alternative to the Lodders (2004) model, we suggest that the high [C]/[O] for WASP-12b arose because the primordial disk was depleted in oxygen abundance during the giant planet's migration. The carbon compounds (CH_4, CO) may have been trapped in ices in the form of planetesimals and then accreted onto the envelope of the gas giant, resulting in the observed enhancement of [C]/[O] > 1. Assuming that the disk started with solar elemental abundances of carbon (2.26×10^{-4}) and oxygen (4.20×10^{-4}), in order to obtain [C]/[O] $= 1.08$ in WASP-12b (our high [C]/[O] model case), the [O] abundance in the disk must have been depleted by $\approx$50%. Recently, Madhusudhan et al. (2011b) performed a more detailed analysis of the formation of WASP-12b and concluded that the primordial disk was depleted in [O] by 41%. The discrepancy in our numbers arises because Madhusudhan et al. (2011b) used elemental abundances of the host star WASP-12 (Fossati et al. 2010), which are 3.54×10^{-4} and 7.94×10^{-4} for [C] and [O], respectively.

It is possible that the depletion of [O] in WASP-12b occurred because the host star accreted fractionated refractory materials (that trapped 41% of [O], in the WASP-12 case) from the protoplanetary disk during planetary formation. In our solar system, planetary migration could have affected giant planet composition to some extent, as Jupiter and Saturn, in particular, are thought to have moved around considerably during planetary accretion (Tsiganis et al. 2005; Gomes et al. 2005; Morbidelli et al. 2005; Walsh et al. 2011), with Jupiter perhaps coming as close in as 1.5 AU. But, as far as we know, giant planets never migrated through the terrestrial planet region of our system. By contrast, in the WASP-12 system, planetary migration was evidently much more pronounced. WASP-12b migrated from the outer parts of the nebula to its present location close to the star. Meanwhile, rocky planets formed in the hot, inner parts of the nebula may have migrated in even closer and have been consumed by the star. If WASP-12b accreted additional material during its journey, that material would have been depleted in O relative to C, possibly accounting for the high [C]/[O] ratio of the planet. Madhusudhan et al. (2011b) mention this possibility, but they rule it out because they argue this would require that [C]/[H] in the envelope of WASP-12b should be close to the host star's value, which is not the case. We do not agree with this objection, however, because all known planets accrete elements heavier than He more efficiently than they do H. Jupiter, for example, is enriched in C, N, and S compared to the Sun by a factor of three (Beatty 1999). Further observations may be needed to determine the validity of this mechanism.

The accretion of refractory elements onto a star has been proposed as one of the reasons why solar twins and analogs in the solar neighborhood have enhanced heavy elemental abundances compared to the Sun (Meléndez et al. 2009; Ramírez et al. 2009). These studies found that the abundances of heavy elements in these solar analog stars increase with their condensation temperature. The authors attribute the apparent depletion of refractory elements in the Sun to the existence of terrestrial planets, and they suggest that Sun accreted refractory-depleted material from the nebula during the formation of the solar system.[12] Indeed, Chambers (2010) showed that adding 4 $M_\oplus$ of Earth-like and carbonaceous-chondrite-like material to the solar convection zone brings the Sun's elemental abundance in line with the mean abundances of solar twins.

Recently, Schuler et al. (2011) derived precise elemental abundances for ten stars using high-resolution spectroscopy. All ten of their stars have at least one giant planet around them at different orbital distances. Their analysis indicated that four stars, all of which have hot Jupiters ($\sim$0.05 AU), show positive correlations between refractory elemental abundance and condensation temperature. This implies that these stars may have accreted refractory-rich planetary material or cores. If a similar accretion happened during the formation of the WASP-12 system, then "pollution" signatures in the atmosphere of WASP-12 may be observable. Formation models of protostars from molecular clouds (Wuchterl & Tscharnuter 2003) indicate that solar-mass protostars have thin convective envelopes ($\sim$0.02 $M_\odot$), similar to the present day Sun, and hence mixing of deposited material may not be significant. But it has been suggested that WASP-12b may be losing mass to its star (Li et al. 2010). If this is the case, then it could be difficult to determine how much of the refractory material has accreted onto WASP-12 during its formation. Fossati et al. (2010) performed a detailed spectropolarimetric analysis of WASP-12 to look for pollution signatures due to the material lost by WASP-12b. They found hints of pollution but were unable to draw firm conclusions. A differential analysis of WASP-12 twins (with the same effective temperature, age, and metallicity), identifying their abundances with high precision, is required to determine if the refractory elemental abundance of WASP-12 does indeed increase with condensation temperature.

5. CONCLUSIONS

In this study, we analyzed how a disequilibrium mechanism such as photochemistry can affect the observed abundances of H_2O, CO, CO_2, and CH_4 in the WASP-12b atmosphere.

[11] It should be noted that, because the base level of the water clouds was not determined, the water abundance in the deep well-mixed regions of Jupiter is still unknown. However, this does not change the observed result that the mixing ratio of H_2O gradually increases with depth.

[12] Note that the accreted material is not depleted in elements such as carbon because they have low condensation temperatures and so did not condense in the inner part of the solar nebula.

We considered two models with [C]/[O] = 0.54 (solar) and [C]/[O] = 1.08 (twice solar). Although our photochemical results agree that high [C]/[O] is needed to explain the observed high abundance of CH_4 and lack of observable H_2O, they also indicate C_2H_2 and HCN are more abundant than CH_4 and should be taken into consideration in modeling hot-Jupiter atmospheres.[13] More importantly, our results indicate that C_2H_2 is the dominant absorber at 1.6 and 8 μm in WASP-12b's atmosphere and the absorption features may possibly be arising from C_2H_2 rather than CH_4. Observations with *Hubble Space Telescope's* WFC3 can resolve this discrepancy.

We also propose a possible mechanism for the origin of the excess carbon observed in WASP-12b. Following other authors, we suggest that WASP-12 may have accreted rocky, O-rich material from the nebula during the formation of the system, leaving the disk relatively enriched in other volatiles such as C and N. WASP-12b then accreted some of this high [C]/[O] material, which thereby gave rise to the high [C]/[O] ratio of the planet. Testing this hypothesis requires that we understand whether WASP-12 is currently stealing mass from its planet, WASP-12b. A high-precision abundance analysis of WASP-12 twins and analogs can shed light on the refractory elemental abundance of WASP-12 and the possible origin of excess carbon in WASP-12b.

The authors thank the referee, Julianne Moses, for pointing out to us the importance of C_2H_2 and HCN chemistry and for in-depth analysis of our work which helped in improved photochemical models and our current manuscript. R.K. and J.F.K gratefully
acknowledge funding from NASA Astrobiology Institute's Virtual Planetary Laboratory lead team, supported by NASA under cooperative agreement NNH05ZDA001C, and the Penn State Astrobiology Research Center.

REFERENCES

Agol, E., Steffen, J., Sari, R., & Clarkson, W. 2005, MNRAS, 359, 567
Asplund, M., Grevesse, N., & Sauval, A. 2005, in ASP Conf. Ser. 336, Cosmic Abundances as Records of Stellar Evolution and Nucleosynthesis, ed. T. G. Barnes, III & F. N. Bash (San Francisco, CA: ASP), 2538
Atreya, S. K., & Wong, A. 2005, Space Sci. Rev., 116, 121
Atreya, S. K., Wong, M. H., Owen, T. C., et al. 1999, Planet. Space Sci., 47, 1243
Banks, P. M., & Kockarts, G. 1973, Aeronomy (New York: Academic)
Baulch, D. L., Cobos, C. J., Cox, R. A., et al. 1992, J. Phys. Chem. Ref. Data, 21, 411
Beatty, J. K. 1999, The New Solar System (Massachusetts: Cambridge Univ. Press)
Burrows, A., Marley, M., Hubbard, W. B., et al. 1997, ApJ, 491, 856
Chambers, J. E. 2010, ApJ, 724, 92
Charbonneau, D., Allen, L. E., Megeath, S. T., et al. 2005, ApJ, 626, 523
Charbonneau, D., Berta, Z. K., Irwin, J., et al. 2009, Nature, 462, 891
Charbonneau, D., Brown, T. M., Latham, D. W., & Mayor, M. 2000, ApJ, 529, L45
Charbonneau, D., Brown, T. M., Noyes, R. W., & Gilliland, R. L. 2002, ApJ, 568, 377
Chase, M. W., Jr. 1998, NIST-JANAF Themochemical Tables, 4th ed., J. Phys. Chem. Ref. Data, Monograph 9, 1-1951
Cobos, C. J., & Troe, J. 1985, J. Chem. Phys., 83, 1010
Collier-Cameron, A. 2002, Astron. Geophys., 43, 421
Cooper, C. S., & Showman, A. P. 2006, ApJ, 649, 1048
Croll, B., Lafreniere, D., Albert, L., et al. 2011, AJ, 141, 30
Deming, D., Seager, S., Richardson, L. J., & Harrington, J. 2005, Nature, 434, 740
Fortney, J. J., Marley, M. S., Lodders, K., Saumon, D., & Freedman, R. 2005, ApJ, 627, 69
Fossati, L., Bagnulo, S., Elmasli, A., et al. 2010, ApJ, 720, 872
Gray, D. 1992, The Observation and Analysis of Stellar Photospheres (2nd ed.; Cambridge: Cambridge Univ. Press)
Gierasch, P. J., Ingersoll, A. P., Banfield, D., et al. 2000, Nature, 403, 628
Gomes, R., Levison, H. F., Tsiganis, K., & Morbidelli, A. 2005, Nature, 435, 466
Hebb, L., Collier-Cameron, A., Loeillet, B., et al. 2009, ApJ, 693, 1920
Henry, G. W., Marcy, G. W., Butler, R. P., & Vogt, S. S. 2000, ApJ, 529, L41
Holman, M. J., & Murray, N. W. 2005, Science, 307, 1288
Ingersoll, A. P., et al. 2000, Science, 403, 630
Javoy, S. 2003, Exp. Thermal Fluid Sci., 27, 371
Kasting, J. F. 1982, J. Geophys. Res., 87, 3091
Kasting, J. F. 1990, Orig. Life Evol. Biosph., 20, 199
Kasting, J. F., Zahnle, K. J., Walker, J. C. G., et al. 1983, Precambrian Res., 20, 121
Kuntson, H. A., Charbonneau, D., Allen, L. E., et al. 2007, Nature, 447, 183
Laughlin, G., Marcy, G. W., Vogt, S. S., Fischer, D. A., & Butler, R. P. 2005a, ApJ, 629, L121
Laughlin, G., Wolf, A., Vanmunster, T., et al. 2005b, ApJ, 621, 1072
Léger, A., Rouan, D., Schneider, J., et al. 2009, A&A, 506, 287
Li, S-L., Miller, N., Lin, D. N. C., et al. 2010, Nature, 463, 1054
Liang, M. C., Parkinson, C. D., Lee, A. Y.-T., Yung, Y. L., & Seager, S. 2003, ApJ, 596, L247
Line, M. R., Liang, M. C., Yung, Y. L., et al. 2010, ApJ, 717, 496
Lodders, K. 2004, ApJ, 611, 587
Madhusudhan, N., Harrington, J., Stevenson, K. B., et al. 2011a, Nature, 469, 64
Madhusudhan, N., Mousis, O., Johnson, T. V., & Lunine, J. I. 2011b, arXiv:1109.3183
Marley, M. S., Fortney, J. J., Hubickyj, O., Bodenheimer, P., & Lissauer, J. J. 2007, ApJ, 655, 541
Mazeh, T., Naef, D., Torres, G., et al. 2000, ApJ, 532, L55
Meléndez, J., Asplund, M., Gustafsson, B., et al. 2009, ApJ, 704, L66
Morbidelli, A., Levison, H. F., Tsiganis, K., & Gomes, R. 2005, Nature, 435, 462
Moses, J. I., Visscher, C., Fortney, J. J., et al. 2011, ApJ, 737, 15
Owen, T., Mahaffy, P., Niemann, H. B., et al. 1999, Nature, 402, 269
Pavlov, A., Brown, L., & Kasting, J. F. 2001, J. Geophys. Res., 106, 23267
Pickles, A. J. 1998, PASP, 110, 863
Pollack, J. B., Hubickyj, O., Bodenheimer, P., et al. 1996, Icarus, 124, 62
Prinn, R. G., & Barshay, S. S. 1977, Science, 198, 1031
Ramírez, I., Meléndez, J., Asplund, M., et al. 2009, A&A, 508, L17
Schuler, S. C., Flateau, D., Cunha, K., et al. 2011, ApJ, 732, 55
Seager, S., Richardson, L. J., Hansen, B. M. S., et al. 2005, ApJ, 632, 1122
Showman, A. P., Fortney, J. J., Lian, Y., et al. 2009, ApJ, 699, 564
Snellen, I. A. G., Albrecht, S., de Mooij, E. J. W., & Le Poole, R. S. 2008, A&A, 487, 357
Swain, M. R., Tinetti, G., Vasisht, G., et al. 2009b, ApJ, 704, 1616
Swain, M. R., Vasisht, G., Tinetti, G., et al. 2009a, ApJ, 690, L114
Tinetti, G., Vidal-Madjar, A., Liang, M.-C., et al. 2007, Nature, 448, 169
Tsang, W., & Hampson, R. F. 1986, J. Phys. Chem. Ref. Data, 15, 1087
Tsiganis, K., Gomes, R., Morbidelli, A., & Levison, H. F. 2005, Nature, 435, 459
Vidal-Madjar, A., Désert, J.-M., Lecavelier des Etangs, A., et al. 2004, ApJ, 604, L69
Vidal-Madjar, A., Lecavelier des Etangs, A., Désert, J.-M., et al. 2003, Nature, 422, 143
Visscher, C., & Moses, J. 2011, ApJ, 738, 72
Walsh, K. J., Morbidelli, A., Raymond, S. N., et al. 2011, Nature, 475, 206
Wuchterl, G., & Tscharnuter, W. M. 2003, A&A, 398, 1081
Youdin, A. N., & Mitchell, J. L. 2010, ApJ, 721, 1113
Yung, L. Y., & DeMore, W. B. (ed.) 1999, Photochemistry of Planetary Atmospheres (New York: Oxford Univ. Press)
Zahnle, K. 1986, J. Geophys. Res., 91, 2819
Zahnle, K., Marley, M. S., & Fortney, J. J. 2009a, arXiv:0911.0728
Zahnle, K., Marley, M. S., Freedman, R. S., Lodders, K., & Fortney, J. J. 2009b, ApJ, 701, L20

[13] Note that this prediction is not specifically a result of our photochemical model, as our thermodynamic equilibrium models predict this, as well.